Published OnlineFirst March 1, 2013; DOI: 10.1158/2159-8290.CD-12-0446

RESEARCH ARTICLE

Coordinate Direct Input of Both KRAS and IGF1 Receptor to Activation of PI3 Kinase in *KRAS*-Mutant Lung Cancer

Miriam Molina-Arcas[1], David C. Hancock[1], Clare Sheridan[1], Madhu S. Kumar[1], and Julian Downward[1,2]

ABSTRACT

Using a panel of non–small cell lung cancer (NSCLC) lines, we show here that MAP-ERK kinase (MEK) and RAF inhibitors are selectively toxic for the *KRAS*-mutant genotype, whereas phosphoinositide 3-kinase (PI3K), AKT, and mTOR inhibitors are not. IGF1 receptor (IGF1R) tyrosine kinase inhibitors also show selectivity for *KRAS*-mutant lung cancer lines. Combinations of IGF1R and MEK inhibitors resulted in strengthened inhibition of *KRAS*-mutant lines and also showed improved effectiveness in autochthonous mouse models of *Kras*-induced NSCLC. PI3K pathway activity is dependent on basal IGF1R activity in *KRAS*-mutant, but not wild-type, lung cancer cell lines. KRAS is needed for both MEK and PI3K pathway activity in *KRAS*-mutant, but not wild-type, lung cancer cells, whereas acute activation of KRAS causes stimulation of PI3K dependent upon IGF1R kinase activity. Coordinate direct input of both KRAS and IGF1R is thus required to activate PI3K in *KRAS*-mutant lung cancer cells.

SIGNIFICANCE: It has not yet been possible to target RAS proteins directly, so combined targeting of effector pathways acting downstream of RAS, including RAF/MEK and PI3K/AKT, has been the most favored approach to the treatment of *RAS*-mutant cancers. This work sheds light on the ability of RAS to activate PI3K through direct interaction, indicating that input is also required from a receptor tyrosine kinase, IGF1R in the case of *KRAS*-mutant lung cancer. This suggests potential novel combination therapeutic strategies for NSCLC. *Cancer Discov; 3(5); 548–63. ©2013 AACR.*

See related commentary by Chen and Sweet-Cordero, p. 491.

Authors' Affiliations: [1]Signal Transduction Laboratory, Cancer Research UK London Research Institute; and [2]Lung Cancer Group, Division of Cancer Biology, The Institute of Cancer Research, London, United Kingdom

Note: Supplementary data for this article are available at Cancer Discovery Online (http://cancerdiscovery.aacrjournals.org/).

M. Molina-Arcas and D.C. Hancock contributed equally to this work.

Corresponding Author: Julian Downward, Cancer Research UK London Research Institute, Signal Transduction Lab, 44 Lincoln's Inn Fields, London WC2A 3PX, United Kingdom. Phone: 011-44-20-7269-3533; Fax: 011-44-20-7269-3094; E-mail: julian.downward@cancer.org.uk

doi: 10.1158/2159-8290.CD-12-0446

Published OnlineFirst March 1, 2013; DOI: 10.1158/2159-8290.CD-12-0446

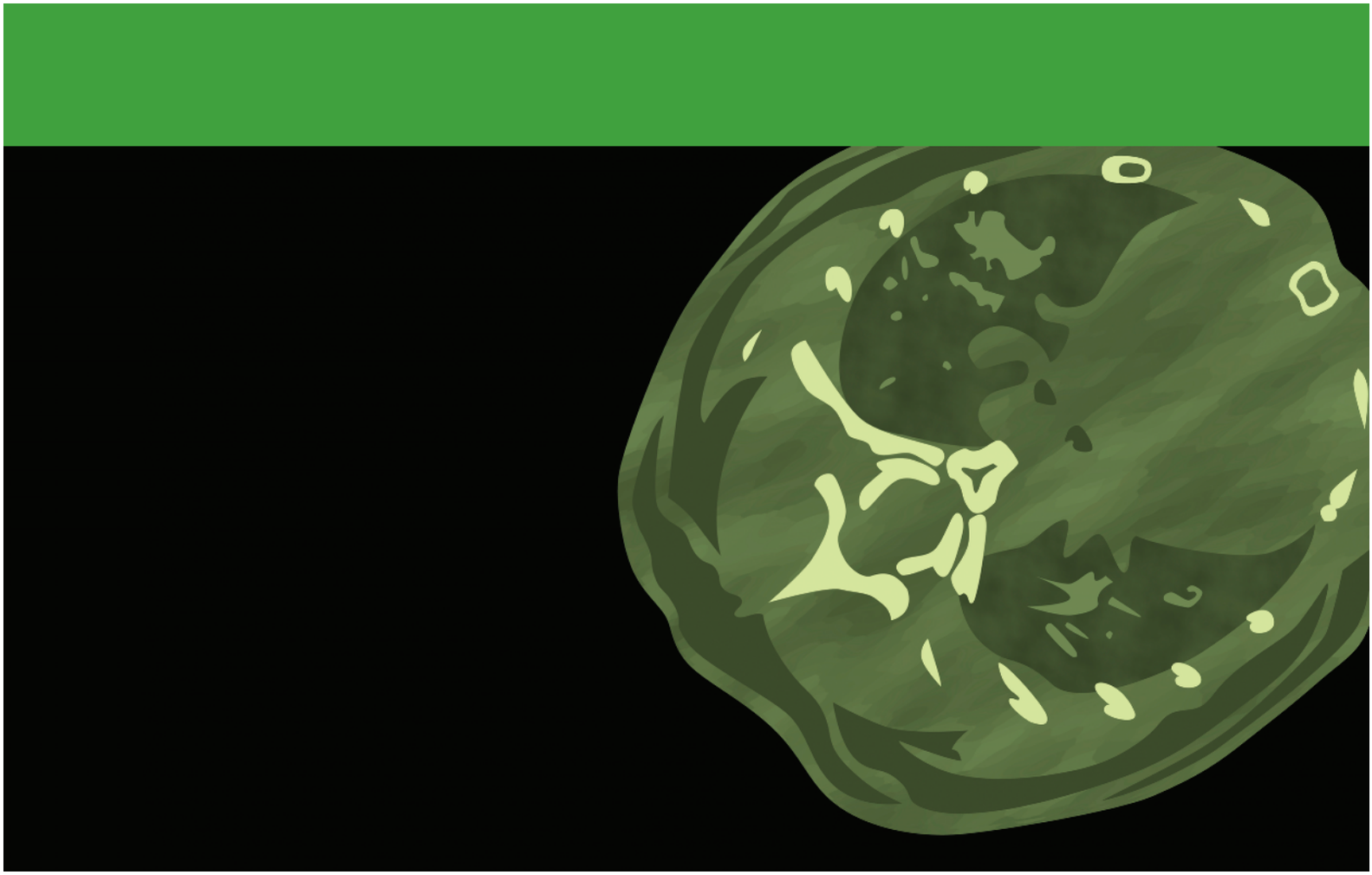

INTRODUCTION

Activating point mutations in the genes encoding the RAS subfamily of small GTP-binding proteins contribute to the formation of a large proportion of human tumors. In lung cancer, one of the most prevalent cancer types worldwide (1), *KRAS* is mutationally activated in approximately 25% of adenocarcinomas (2, 3). This poses a significant therapeutic challenge, as *KRAS* mutations are generally associated with resistance to existing therapies (4, 5). Targeting RAS itself presents an attractive approach to this issue, as *RAS*-mutant tumors have been shown to exhibit oncogene addiction (6, 7). However, in contrast to the efficacy of tyrosine kinase inhibitors in patients with mutant receptor tyrosine kinases (RTK), pharmacologic targeting of activated RAS proteins has been unsuccessful to date. Thus, efforts have shifted toward targeting pathways acting downstream of RAS. Indeed, combined inhibition of extracellular signal-regulated kinase (ERK) and phosphoinositide 3-kinase (PI3K) signaling, 2 well-described RAS-controlled pathways, has shown some efficacy in mutant *Kras*-driven mouse lung tumor models (8). This combination of pathway inhibitory drugs is being explored in a number of early-phase clinical trials, but so far, both the toxicity and efficacy of this approach is unclear.

Tumors with *RAS* mutations can also show selective dependencies on activities that are not regulated directly by RAS. To identify factors or pathways necessary for survival and proliferation of cells harboring *KRAS* mutations, several groups have conducted synthetic lethal RNA interference (RNAi) screens. The list of candidates obtained thus far includes the TANK-binding kinase 1 (TBK1; ref. 9), the transforming growth factor β–activated kinase 1 (TAK1; ref. 10), the transcription factor GATA2 (11, 12), the G_1–S regulator cyclin-dependent kinase 4 (CDK4; ref. 13), mitotic regulators (14), and proteasome components (12, 14). Differences in cell type and in specific assay conditions may help explain some of the variability across these different datasets and deeper investigation is required to understand the broader significance of these factors in RAS-driven tumors. Crucially, most of these screens have identified candidate novel targets for drug development, meaning that a significant period must inevitably elapse until any such potential therapy reaches clinical trials. Thus, a complementary approach is to identify targets that are necessary for survival of *RAS*-mutant cells using compounds that are already available and/or in clinical use. The use of drugs in RAS synthetic lethal screening can permit the analysis of a larger panel of cells, help avoid some of the off-target effects associated with RNA interference (RNAi) and, more importantly, identify immediately applicable therapeutic strategies to treat *RAS*-mutant tumors.

In this study, we have assayed a collection of small-molecule inhibitors on a panel of human lung cancer cell lines to identify drugs that show selectivity for the *KRAS*-mutant genotype. Cells harboring *KRAS* mutations were found to be more sensitive than *KRAS* wild-type cells to inhibition of the RAF/mitogen-activated protein (MAP)-ERK kinase (MEK)/ERK pathway, whereas no *KRAS* genotype selectivity was observed when the PI3K/AKT/mTOR pathway was inhibited. Interestingly, however, *KRAS*-mutant cells exhibit increased dependence on the activity of the insulin-like growth factor 1 receptor (IGF1R). Mechanistically,

Published OnlineFirst March 1, 2013; DOI: 10.1158/2159-8290.CD-12-0446

we show that the ability of KRAS to directly activate the PI3K activity of the p110 catalytic subunit requires a coordinate input from an RTK, IGF1R in the case of lung cancer, acting via the p85 regulatory subunit. These findings suggest potential therapeutic strategies for lung tumors harboring *KRAS* mutations while avoiding the potential toxicities of direct PI3K inhibition.

RESULTS

KRAS-Mutant NSCLC Cell Lines Are Selectively Sensitive to MEK, RAF, and IGF1R Inhibitors

Using a collection of small-molecule inhibitors, we aimed to identify pathways that are critical for the maintenance and survival of tumor cells carrying an activating *KRAS* mutation, but not to those lacking this oncogene. For this purpose, we assembled a panel of 25 non–small cell lung cancer (NSCLC) cell lines, 13 of which are *KRAS* mutant and 12 *KRAS* wild-type (Supplementary Table S1). Cell lines known to harbor epidermal growth factor receptor (*EGFR*) mutations were purposely excluded from the selection. To conduct an initial characterization of the dependence of the 2 groups on the expression of KRAS for cell survival, we used RNA interference to deplete endogenous levels of *KRAS* acutely. As anticipated, *KRAS* knockdown using 2 different siRNA pools led to a notable selective increase in apoptosis in most of the *KRAS*-mutant, but not wild-type, cells and an accompanying decrease in cell viability (Fig. 1A and B). This effect was more statistically significant using siRNAs that have been chemically modified to reduce off-target effects (OTP; ref. 15) and indicates that most of the *KRAS*-mutant cell lines in this panel show some evidence of RAS oncogene addiction.

Next, we used the panel of 25 NSCLC cell lines to assess the effect on cell viability of more than 50 small-molecule inhibitors targeting pathways directly controlled by RAS, such as RAF/MEK/ERK or PI3K/AKT/mTOR, as well as drugs directed against other less direct targets such as HSP90 or NF-κB. Figure 1C–J and Supplementary Fig. S1A and S1B illustrate the effect on cell viability of several selected inhibitors. To identify those drugs achieving statistical significance in discriminating between *KRAS*-mutant and wild-type cells, we conducted two-way ANOVA (Table 1). The analysis revealed that cells bearing *KRAS* mutations tended to be, as expected (16), significantly more sensitive to RAF and MEK inhibitors than *KRAS* wild-type cells. Of the RAF inhibitors, AZ628 showed the greatest selectivity; this is a pan-RAF inhibitor with somewhat more potency towards CRAF (29 nmol/L) than BRAF (110 nmol/L; ref. 17). However, no significant *KRAS* genotype selectivity was observed when the PI3K/AKT/mTOR pathway was inhibited by any of a range of targeted molecules, with considerable loss of cell viability seen on most cell lines irrespective of genotype. Intriguingly, *KRAS*-mutant cells exhibited enhanced sensitivity to a different class of drugs, 3 of the 5 tested IGF1R inhibitors. Indeed, *p* values associated with these 3 drugs were among the most significant, comparing favorably with those produced by the most potent MEK inhibitors. In contrast, although values failed to reach statistical significance, *KRAS* wild-type cells tended to show increased sensitivity toward EGFR inhibition compared with mutant cells. Finally, cells carrying *KRAS* mutations also responded slightly more strongly to the HSP90 inhibitors 17-AAG and 17-DMAG and to the MET/ALK kinase inhibitor PF-02341066, although the magnitude of these effects was considerably less than for the best MEK, RAF, and IGF1R inhibitors. Rho kinase (ROCK) and proteasome inhibitors did not show selectivity as single agents, although combination inhibition of these pathways is selectively toxic for *KRAS*-mutant cells, especially *in vivo* (11, 12). As illustrated in the viability graphs in Fig. 1 and Supplementary Fig. S1, drugs directed against the same target tend to cluster together in a heatmap analysis (Supplementary Fig. S1C), providing a degree of reassurance with respect to the reproducibility and on-target nature of these differential effects.

In summary, we found that NSCLC cells harboring a *KRAS*-mutant allele are, in general, more sensitive to MEK, RAF, and IGF1R inhibitors than cells with wild-type *KRAS*. No obvious differences were seen in this between the different amino acid changes at codons 12, 13, or 61 in the *KRAS*-mutant cell lines used.

IGF1R Inhibitors Selectively Inhibit AKT Activation in *KRAS*-Mutant NSCLC Cells

To investigate the mechanistic basis for the different response of NSCLC cell lines to MEK and IGF1R inhibitors, we examined the effect of these compounds on the activity of the MEK/ERK and PI3K/AKT pathways. As expected, we observed efficient reduction of ERK phosphorylation upon treatment with the MEK inhibitor PD-0325901 across the entire cell panel (Fig. 2A and Supplementary Fig. S2). In addition, there was a modest and persistent increase in AKT phosphorylation in both genotypes, probably due to suppression of well-characterized negative feedback loops (18–20). Interestingly, MEK inhibition in *KRAS*-mutant, but not wild-type, cells produced a striking reduction in ribosomal protein S6 phosphorylation, an indirect measure of mTOR complex 1 (mTORC1) activity, which became evident at later time points, possibly indicating a more indirect mechanism. Consistent with this finding, we also found reduced phosphorylation on Thr389 of the direct mTORC1 substrate p70 ribosomal protein S6 kinase (p70S6K) after MEK inhibitor treatment of *KRAS*-mutant cells.

In response to IGF1R inhibition by NVP-AEW541, cells harboring a *KRAS* mutation showed an early, marked suppression of AKT phosphorylation that was sustained at 24 hours (Fig. 2B and Supplementary Fig. S3A). Consistent with this finding, there was a strong reduction in phosphorylation of the AKT substrate PRAS40 on Thr246. Notably, these effects were not evident in *KRAS* wild-type cells, even though treatment with AKT or PI3K inhibitors produced the same level of reduction in AKT phosphorylation in both *KRAS*-mutant and wild-type cells (Supplementary Fig. S3B). These data suggest that inhibition of IGF1R has a clear impact upon the reduction of PI3K activity only in the cells carrying a *KRAS* mutation. Moreover, the change in AKT phosphorylation seen at 4 hours after NVP-AEW541 treatment correlated strongly with the effect on cell viability after a 72-hour treatment (Fig. 2B, right). Thus, the differences in the reduction of AKT phosphorylation may provide an explanation as to why *KRAS*-mutant NSCLC cells are more sensitive to IGF1R inhibition.

Combining IGF1R Inhibitors with MEK Inhibitors Enhances Their Differential Impact upon Mutant *KRAS*–Driven Lung Cancer

The data presented above show that *KRAS*-mutant NSCLC cells are preferentially sensitive to inhibition of both

Published OnlineFirst March 1, 2013; DOI: 10.1158/2159-8290.CD-12-0446

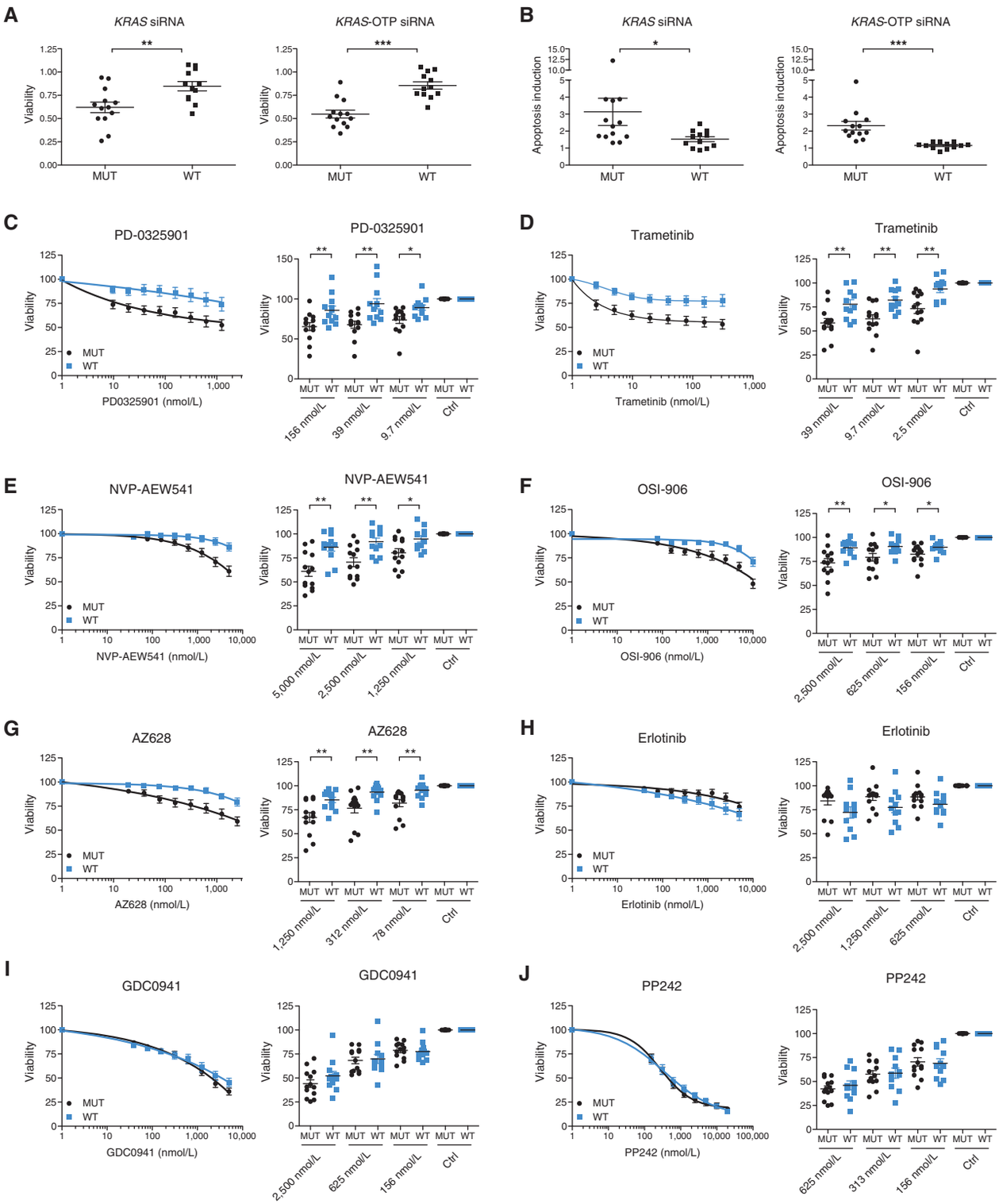

Figure 1. *KRAS*-mutant NSCLC cells are selectively sensitive to MEK, RAF, and IGF1R inhibitors. **A** and **B,** twenty-five NSCLC cell lines (13 *KRAS*-mutant and 12 *KRAS* wild-type) were transfected with *KRAS*, *KRAS*-OTP, or control siRNAs. Relative cell viability (**A**) and apoptosis (**B**) were measured 96 hours after transfection. **C–J,** twenty-five NSCLC cell lines were treated for 72 hours with serial dilutions of MEK (**B** and **C**), IGF1R (**E** and **F**), RAF (**G**), EGFR (**H**), PI3K (**I**), and mTOR (**J**) inhibitors. Left, curves representing average values for each *KRAS* genotype (mean ± SEM). Right, single data points representing individual cell lines at 3 selected drug doses. MUT, mutant; WT, wild-type.

Published OnlineFirst March 1, 2013; DOI: 10.1158/2159-8290.CD-12-0446

Table 1. Drugs tested in the panel of 25 NSCLC cell lines

			Two-way ANOVA (MUT vs. WT)		
	Drug	Target	Dose range (nmol/L)	*P*	Significance
RAF/MEK/ERK	**Trametinib**	MEK	1,250–9.76	0.0031	**
	PD-0325901	MEK	1,250–9.76	0.0053	**
	Selumetinib	MEK	1,250–9.76	0.0181	*
	CI-1040	MEK	1,250–9.76	0.0123	*
	AZ628	RAF	2,500–19.5	0.0037	**
	L779450	RAF	20,000–156	0.0274	*
	PLX4720	RAF	20,000–156	0.0116	*
	GDC-0879	RAF	20,000–156	0.0483	*
	Sorafenib	RAF	10,000–78	0.0285	*
	ZM336372	RAF	20,000–156	0.0924	ns
	GW5074	RAF	10,000–78	0.1282	ns
	SB590885	RAF	2,0000–156	0.2135	ns
PI3K/AKT/mTOR	GDC0941	PI3K	5,000–39	0.6078	ns
	PIK-90	PI3K	2,500–19.5	0.7292	ns
	PIK-75	PI3K (p110α)	250–1.95	0.2477	ns
	NVP-BEZ235	PI3K/mTOR	250–1.95	0.2202	ns
	PF-04691502	PI3K/mTOR	5,000–39	0.9707	ns
	PP242	mTOR (kinase)	2,0000–156	0.6741	ns
	AZD8055	mTOR (kinase)	5,000–39	0.5811	ns
	Everolimus	mTOR (rapalog)	5,000–39	0.8585	ns
	Temsirolimus	mTOR (rapalog)	5,000–39	0.9338	ns
	Akti- 1/2	AKT	20,000–156	0.2065	ns
	MK-2206	AKT	20,000–156	0.9727	ns
RTK	**NVP-AEW541**	IGF1R	5,000–39	0.0042	**
	OSI-906	IGF1R	10,000–78	0.0041	**
	BMS-754807	IGF1R	5,000–39	0.0014	**
	Picropodophyllin	IGF1R	1,000–7.8	0.4921	ns
	IGF-1R Inhibitor II	IGF1R	20,000–156	0.5752	ns
	Erlotinib	EGFR	5,000–39	0.1073	ns
	Gefitinib	EGFR	5,000–39	0.0139	ns
OTHER	**17-AAG**	HSP90	500–3.9	0.0355	*
	17-DMAG	HSP90	500–3.9	0.0401	*
	BIIB021	HSP90	500–3.9	0.1456	ns
	NVP-AUY922	HSP90	500–3.9	0.5857	ns
	BX-795	TBK1	5,000–39	0.1786	ns
	PF-02341066	c-Met	5,000–39	0.0479	*
	SU11274	c-Met	5,000–39	0.4032	ns
	Bortezomib	Proteasome	250–1.95	0.406	ns
	MG-132	Proteasome	5,000–39	0.3896	ns
	PSI	Proteasome	2,500–19.5	0.8714	ns
	Doxorubicin	Topoisomerase	1,125–8.9	0.1158	ns
	Topotecan	Topoisomerase	2,500–19.5	0.4927	ns
	BMS-345541	IKK-β	20,000–156	0.3172	ns
	SC-514	IKK-2	20,000–156	0.9998	ns
	CAY10576	IKK-e	20,000–156	0.5216	ns
	5Z-7-Oxozeaenol	TAK1 (NF-κB)	20,000–156	0.2505	ns
	Fasudil	ROCK	20,000–156	0.8516	ns
	Y-27632	ROCK	20,000–156	0.9011	ns
	Docetaxel	Microtubule	10–0.078	0.3609	ns
	MK2a Inhibitor	MK2	5,000–39	0.1352	ns
	Deguelin	MT-bioenergetics	20,000–156	0.7901	ns
	10058-F4	c-Myc	20,000–156	0.2072	ns
	PF-573,228	FAK	20,000–156	0.4752	ns
	GDC-0449	Hedgehog pathway	20,000–156	0.6057	ns
	Dasatinib	SRC	5,000–39	0.1236	ns

NOTE: Cell viability was measured across an 8-point titration range. Two-way ANOVA was used to examine significant differences in sensitivity between *KRAS*-mutant (MUT) and wild-type (WT) cells. Only primary drug targets are indicated. Abbreviation: ns, not significant.

Published OnlineFirst March 1, 2013; DOI: 10.1158/2159-8290.CD-12-0446

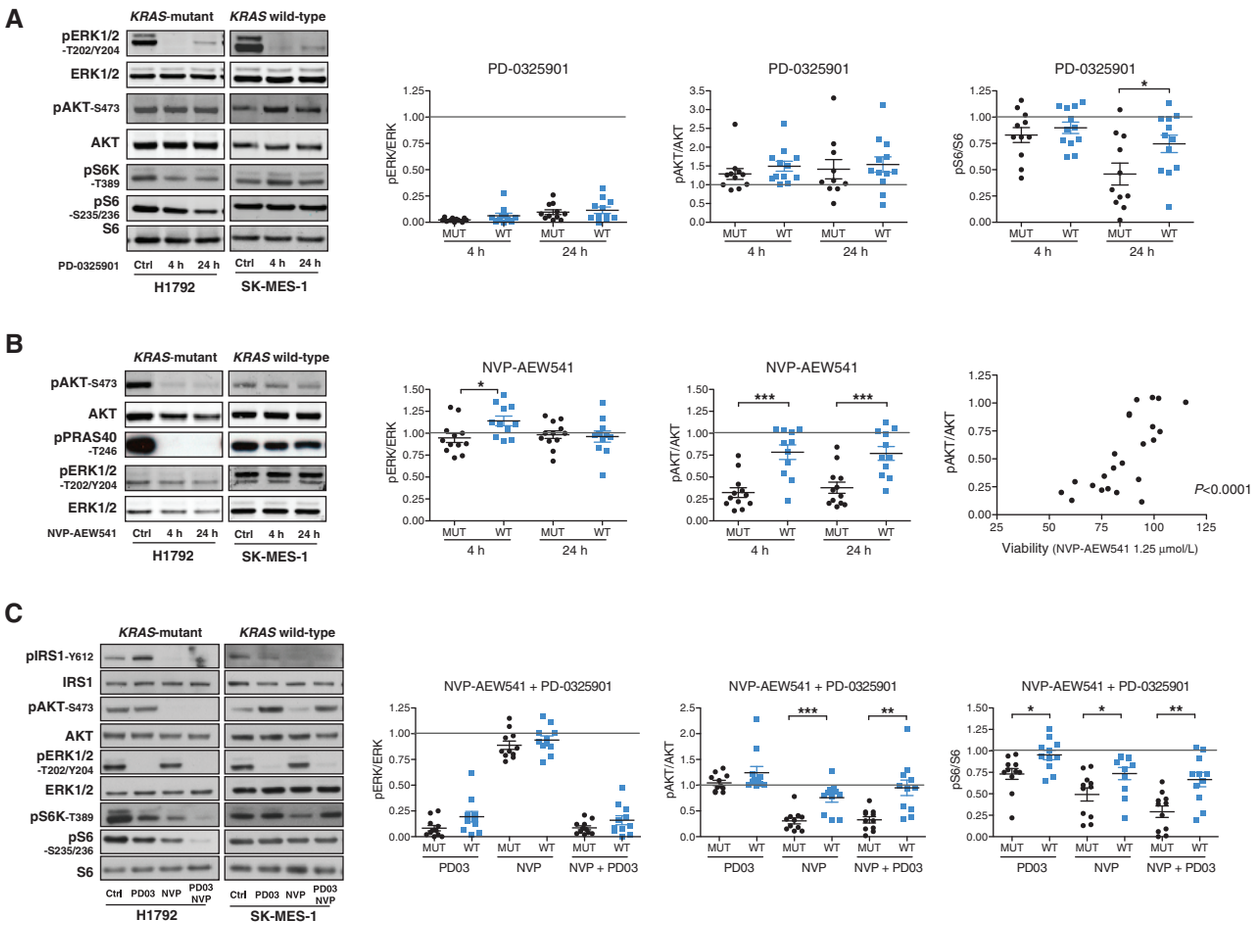

Figure 2. Effects of MEK and IGF1R inhibitors on signal transduction pathways in NSCLC cell lines. **A,** *KRAS*-mutant and *KRAS* wild-type NSCLC cells were treated for 4 or 24 hours with 100 nmol/L PD-0325901, and cell lysates were probed with the indicated antibodies. For all Western blots, see Supplementary Fig. S2. **B,** NSCLC cells were treated for 4 or 24 hours with 1 μmol/L NVP-AEW541, and cell lysates were probed with the indicated antibodies. For all Western blots, see Supplementary Fig. S3A. Right, the correlation between phosphorylated AKT (pAKT)/AKT ratios (at 24 hours) and cell viability (measured at 72 hours) after treatment with 1.25 μmol/L NVP-AEW541. **C,** NSCLC cells were treated for 4 hours with either 1 μmol/L NVP-AEW541, 10 nmol/L PD-0325901, or both together, and cell lysates were probed with the indicated antibodies. For all Western blots, see Supplementary Fig. S4. **A–C,** the levels of phosphorylated ERK (pERK)/total ERK1/2, AKT, and S6 were measured for each cell line by quantitative infrared imaging and normalized to vehicle-treated cells. H1792 and SK-MES-1 cells are displayed as exemplars of each genotype. MUT, mutant; WT, wild-type.

MEK and IGF1R, and that IGF1R inhibition reduces AKT phosphorylation only in *KRAS*-mutant cells. Thus, a combination of both drugs would allow for simultaneous inhibition of the PI3K/AKT and MEK/ERK pathways selectively in *KRAS*-mutant cells and might be expected to increase the differential sensitivity between *KRAS*-mutant and wild-type cells.

To explore this possibility, we examined the effect of a combination of NVP-AEW541 with PD-0325901 upon the activity of MEK/ERK and PI3K/AKT signaling pathways after a 4-hour treatment (Fig. 2C and Supplementary Fig. S4). As expected, this combination decreased ERK phosphorylation in both mutant and wild-type cells with no differences as compared with the effect of MEK inhibitor alone. Moreover, the combination reduced AKT phosphorylation only in *KRAS*-mutant cells with the effects being comparable to those seen with the IGF1R inhibitor alone. Phosphorylation on Tyr612 of the adaptor protein insulin receptor substrate 1 (IRS1) served as an additional monitor of IGF1R pathway inhibition by NVP-AEW541 both alone and in combination. Intriguingly, combined inhibition of MEK and IGF1R led to a more robust inhibition of S6 phosphorylation in *KRAS*-mutant cells. Consistent with this, a corresponding effect was also evident when we looked at phosphorylation of the S6 upstream kinase p70S6K. These data indicate that the combination of MEK and IGF1R inhibitors in *KRAS*-mutant cells causes not only a combined inhibition of PI3K/AKT and MEK/ERK pathways, but also a stronger inhibition of mTORC1 activity.

To assess the effect of drug combinations further, we augmented NVP-AEW541 with low doses of PD-0325901 and found that this reduced cell viability more strongly than single agent in *KRAS*-mutant cells but not in wild-type cells (Supplementary Fig. S5A). This synergistic effect was associated with an increased induction of apoptosis, at least in some cell lines (Supplementary Fig. S5B). Comparison of the IC_{60} values (drug dose leading to 60% survival relative to untreated cells) showed that in most *KRAS*-mutant cells, the combination

Published OnlineFirst March 1, 2013; DOI: 10.1158/2159-8290.CD-12-0446

of NVP-AEW541 with PD-0325901 clearly reduced the IC_{60} value, whereas no significant differences were observed in most *KRAS* wild-type cells (Supplementary Fig. S6A). This increase in the differential effect between *KRAS*-mutant and wild-type cells could be seen across a range of doses of NVP-AEW541 and was also evident when we compared the average response of each *KRAS* genotype (Fig. 3A). Interestingly, the combination of NVP-AEW541 with low doses of the potent pan-RAF inhibitor AZ628 showed similar effects (Fig. 3B). These results could be replicated with an alternative IGF1R inhibitor, OSI-906 (Supplementary Fig. S6C–S6E) and with trametinib (GSK1120212), an alternative MEK inhibitor (Supplementary Fig. S6B and S6F). Furthermore, the combination of IGF1R and MEK inhibitors in a long-term cell-growth assay also showed a strong relative reduction of cell viability in *KRAS*-mutant cells (Supplementary Fig. S6G).

Combination treatment with PI3K and MEK inhibitors has previously shown efficacy in *Kras*-mutant lung tumor mouse models (8). We therefore decided to assess the effect of combining a PI3K inhibitor with low doses of a MEK or RAF inhibitor in the panel of NSCLC cell lines. Although treatment with PI3K inhibitors alone showed no selectivity between wild-type and mutant cells, *KRAS*-mutant cells exhibited enhanced sensitivity to the combination of PI3K and MEK inhibitors (Fig. 3C). The addition of a MEK or RAF inhibitor to the PI3K inhibitor GDC0941 increased the sensitivity of *KRAS*-mutant but not *KRAS* wild-type cells (Fig. 3C and D and Supplementary Fig. S6H–I), but the enhanced genotype-specific differential effect was, in general, less striking than that seen with IGF1R and MEK inhibitor combinations, due mainly to the stronger impact of direct PI3K inhibition on *KRAS* wild-type cells.

The fact that the IGF1R inhibitors used in this study are known to inhibit the closely related insulin receptor (INSR) to varying degrees prompted us to use siRNAs directed against *IGF1R* or *INSR* as a means to assess the effects of abrogating the activity of each receptor individually. Silencing of IGF1R expression in the panel of NSCLC cells led to a significant loss of viability of *KRAS*-mutant cells as compared with *KRAS* wild-type counterparts, whereas knockdown of INSR produced rather minor effects (Fig. 3E). In keeping with our observations using IGF1R inhibitors, IGF1R knockdown strikingly reduced AKT phosphorylation in *KRAS*-mutant cells, with INSR silencing producing no such response (Supplementary Fig. S7A), and the combination of IGF1R knockdown with MEK inhibition augmented the *KRAS*-mutant genotype-specific effect on cell viability (Fig. 3F).

To investigate the possible utility of drug combinations in an *in vivo* setting, we sought to assess the impact of MEK and IGF1R inhibition on the maintenance and progression of *Kras*-driven lung tumors in 2 different autochthonous genetically engineered mouse models. We elected to use trametinib for MEK inhibition due to both its potency at low concentrations *in vitro* (Fig. 1D and Supplementary Fig. S6B, S6F, and G) and its long half-life *in vivo* (21). In addition, alone of the MEK inhibitors, this drug has proven to be effective in a clinical trial on *BRAF*-mutant melanoma (22). Accordingly, $Kras^{LA2\text{-}G12D/+}$ mice (23) were allowed to develop lung tumors that could be readily detected by micro-computerized tomography (CT) scanning. Animals were then treated daily with either vehicle, IGF1R inhibitor NVP-AEW541, MEK inhibitor trametinib, or a combination of both inhibitors, for 6 weeks and were scanned again at the end of the treatment period. The change in volume of individual tumors over time was then evaluated. Individual lung tumors arising in $Kras^{LA2\text{-}G12D/+}$ mice tend to grow relatively slowly and, as anticipated, tumors that were longitudinally tracked in vehicle control-treated animals generally exhibited a modest increase in size over the treatment period. Nevertheless, we observed that tumors in mice treated with individual MEK or IGF1R inhibitors showed a small decrease in mean tumor volume and that this effect was exacerbated when the inhibitors were combined (Fig. 3G). The efficacy of each inhibitor in this *in vivo* context is illustrated in Supplementary Fig. S7B. Analysis of individual tumor nodules at the conclusion of the treatment regime showed that IGF1R inhibition had produced a clear, albeit incomplete, reduction in AKT phosphorylation, and MEK inhibition resulted in the total abrogation of ERK phosphorylation (Supplementary Fig. S7B). To evaluate the effect of MEK and IGF1R inhibition in a more aggressive *Kras*-driven mouse lung tumor model, we inoculated the lungs of $Kras^{LSL\text{-}G12D}$; $Trp53^{Flox/Flox}$ mice with adenovirus-expressing Cre recombinase to induce concomitant activation of oncogenic *KRAS* and deletion of the tumor suppressor p53 (24). Mice were scanned by micro-CT to identify development of individual lung tumors, and tumor-bearing animals were then treated daily with either vehicle, MEK inhibitor trametinib, IGF1R inhibitor OSI-906, or a combination of both inhibitors for 2 weeks. After rescanning at the end of the treatment period, changes in the volume of individual tumors over this time frame were calculated for each group (Fig. 3H). Although tumors that develop in this mouse model tend to grow more rapidly than those in the $Kras^{LA2\text{-}G12D/+}$ model, we observed a similar response to MEK and IGF1R inhibition. Targeting each pathway individually provided some reduction in tumor growth, but inhibiting both pathways simultaneously had a considerably stronger impact. Taken together, our results suggest the combination of IGF1R and MEK inhibitors as a novel potential therapy for *KRAS*-mutant NSCLC.

KRAS-Mutant NSCLC Cells Exhibit Increased Dependence on IGF1R Signaling

The IGF1R pathway is activated by insulin-like growth factors binding to the heterotetrameric IGF1 RTK, resulting in receptor autophosphorylation, binding to the IRS adaptor proteins, IRS protein tyrosine phosphorylation, and subsequent binding to effector enzymes such as the regulatory p85 subunit of PI3K. To investigate the differential effect of IGF1R inhibition on PI3K activity in NSCLC cells, we analyzed the activity of the IGF1R pathway in 12 cell lines, 6 of which are *KRAS*-mutant and 6 *KRAS* wild-type. Cells were serum-starved overnight and then stimulated for 30 minutes with either IGF1 or EGF. A phosphospecific antibody recognizing Tyr612 of the IGF1R adaptor protein IRS1 (and also equivalent Tyr653 on IRS2) was used to measure activation of the IGF1R pathway; these sites, when phosphorylated, bind to p85, leading to PI3K activation. IGF1 stimulation induced a strong increase in phospho-IRS and phospho-AKT in all 6 *KRAS*-mutant cell lines tested, whereas only 3 of 6 wild-type cells showed activation of the IGF1R pathway (Fig. 4A and Supplementary Fig. S8A). As described above,

Published OnlineFirst March 1, 2013; DOI: 10.1158/2159-8290.CD-12-0446

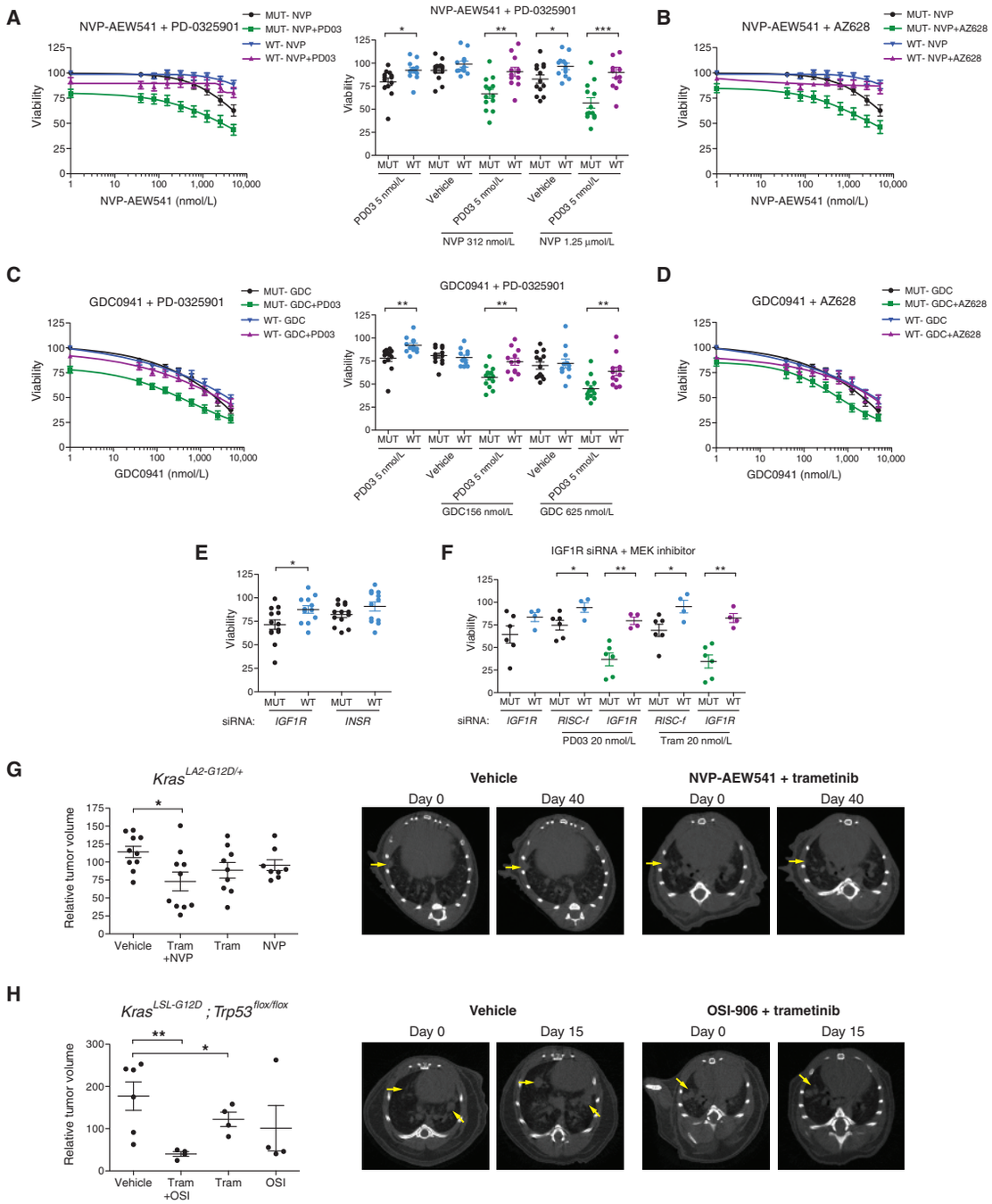

Figure 3. Combining IGF1R inhibitors with MEK or RAF inhibitors enhances the differential impact upon mutant *KRAS* cells. **A–D,** *KRAS*-mutant and *KRAS* wild-type NSCLC cells were treated for 72 hours with serial dilutions of IGF1R inhibitor NVP-AEW541 (**A** and **B**) or PI3K inhibitor GDC0941 (**C** and **D**), together with low doses of MEK (**A** and **C**) or RAF (**B** and **D**) inhibitor (5 nmol/L PD-0325901 or 100 nmol/L AZ628). Curves represent average values for each *KRAS* genotype (mean ± SEM). Right panels of **A** and **C** show single data points representing viability of individual cell lines at 2 representative doses of IGF1R or PI3K inhibitors in the presence or absence of MEK inhibitor PD-0325901. **E,** twenty-five NSCLC cell lines were transfected with *IGFR*, *INSR*, or control siRNAs. Relative cell viability was measured 96 hours after transfection. **F,** six *KRAS*-mutant and 4 *KRAS* wild-type cells were transfected with *IGFR* or control siRNAs and 24 hours later treated with MEK inhibitors (20 nmol/L PD-0325901 or 20 nmol/L trametinib). Relative cell viability was measured 72 hours after drug treatment. **G,** $Kras^{LA2\text{-}G12D/+}$ mice were scanned by micro-CT at 12 weeks of age to identify individual lung tumors. Animals were treated daily for 6 weeks with either vehicle, trametinib (2.5 mg/kg), NVP-AEW541 (50 mg/kg), or a combination of both inhibitors at these doses and then rescanned at the end of this regime. Changes in volume of individual tumors over the treatment period were calculated for each group. Relative transaxial images before and after the treatment are shown. Yellow arrows indicate detectable lesions. **H,** $Kras^{LSL\text{-}G12D}$; $Trp53^{Flox/Flox}$ mice were infected with adenovirus expressing Cre recombinase and were scanned by micro-CT 12 weeks later to identify individual lung tumors. Animals were treated daily for 2 weeks with either vehicle, trametinib (2.5 mg/kg), OSI-906 (40 mg/kg), or a combination of both inhibitors at these doses and then rescanned at the end of this regime. Changes in volume of individual tumors over the treatment period were calculated for each group. Relative transaxial images before and after the treatment are shown. Yellow arrows indicate detectable lesions. MUT, mutant; WT, wild-type.

Published OnlineFirst March 1, 2013; DOI: 10.1158/2159-8290.CD-12-0446

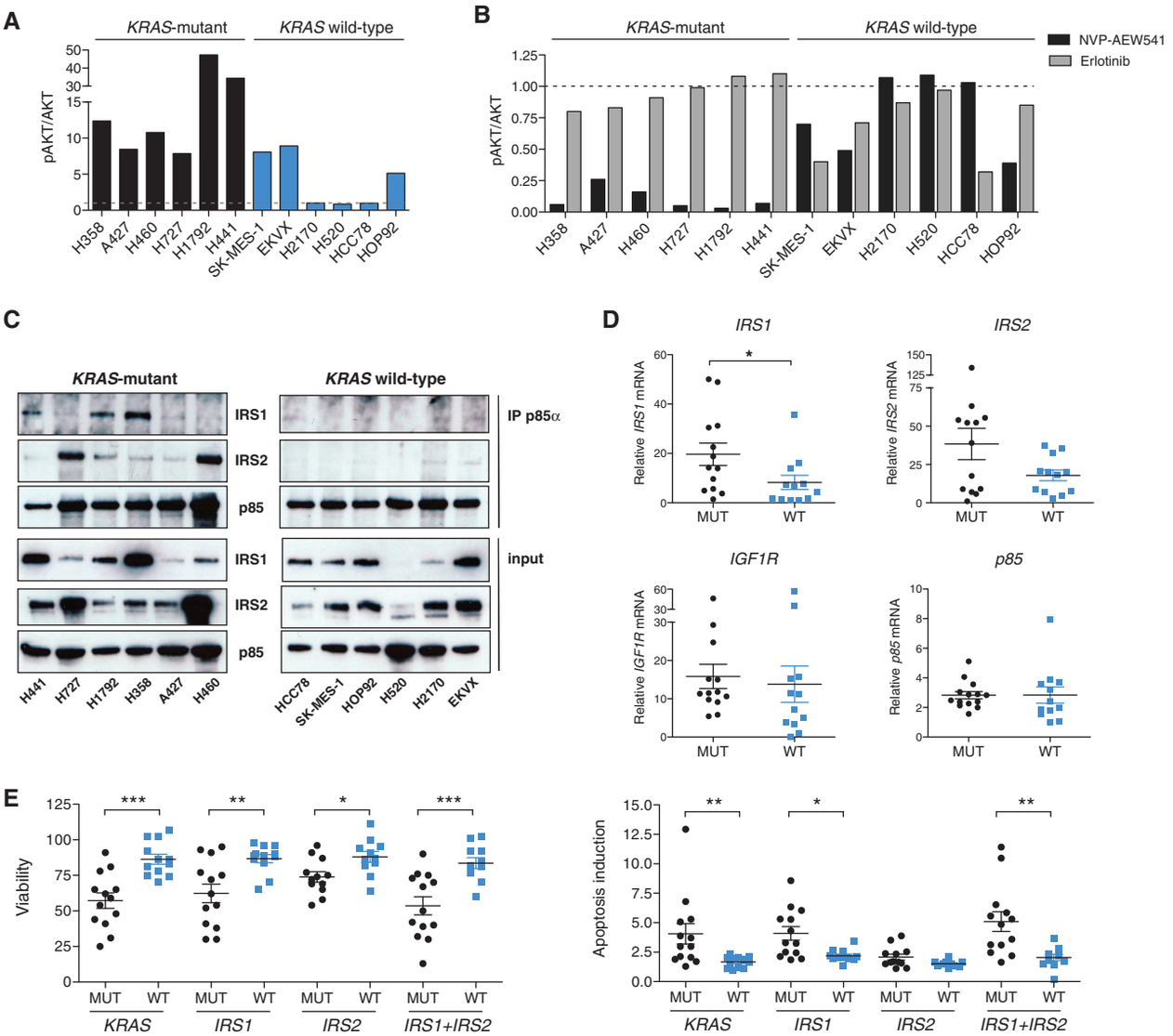

Figure 4. *KRAS*-mutant NSCLC cell lines exhibit dependence upon the IGF1R pathway. **A,** six *KRAS*-mutant and 6 *KRAS* wild-type NSCLC cell lines were deprived of serum for 24 hours and induction of phosphorylated AKT (pAKT)/total AKT was determined following a 30-minute stimulation with 20 ng/mL IGF1. For Western blots, see Supplementary Fig. S8A. **B,** NSCLC cell lines were treated for 4 hours with either 1 μmol/L NVP-AEW541 or 1 μmol/L erlotinib and the levels of pAKT/total AKT were measured. For Western blots, see Supplementary Fig. S8B. **C,** cell extracts from NSCLC cell lines growing at steady state were immunoprecipitated with anti-p85α antibody. Immunoprecipitates and whole-cell lysates were analyzed by immunoblot using IRS1 and IRS2 antibodies. **D,** *IRS1, IRS2, IGF1R,* and *p85α* mRNA levels in the panel of 25 NSCLC cell lines were analyzed by quantitative PCR. *18S* RNA was used as endogenous control. **E,** twenty-five NSCLC cell lines were transfected with *KRAS, IRS1, IRS2, IRS1 + IRS2,* or control siRNAs. Relative cell viability and apoptosis induction were measured 96 hours after transfection. MUT, mutant; WT, wild-type.

cells carrying *KRAS* mutations showed a marked suppression in steady-state AKT phosphorylation in response to IGF1R inhibition by NVP-AEW541; in contrast, treatment with the EGFR inhibitor erlotinib did not affect AKT phosphorylation (Fig. 4B and Supplementary Fig. S8B). *KRAS* wild-type cells showed a higher degree of variability in their responses to IGF1R and EGFR inhibition. IGF1R inhibition decreased phospho-AKT only in the 3 cell lines that were responsive to IGF1 stimulation, although the magnitude of this effect was much less pronounced than in *KRAS*-mutant cells. Moreover, the wild-type cells in general also showed a more prominent decrease in AKT phosphorylation in response to EGFR inhibition. In keeping with these observations, *KRAS*-mutant cells generally expressed higher steady-state levels of phospho-IRS1, whereas *KRAS* wild-type cells had higher levels of phospho-EGFR (Supplementary Fig. S8C). To explore further the activation of PI3K in this collection of NSCLC cell lines, we analyzed the binding of IRS adaptor proteins to p85α. Immunoprecipitation of p85α led to the clear coprecipitation of IRS1 and/or IRS2 in the *KRAS*-mutant cells, whereas coprecipitation of either of these IRS proteins from *KRAS* wild-type cells was barely detectable

Published OnlineFirst March 1, 2013; DOI: 10.1158/2159-8290.CD-12-0446

(Fig. 4C). Taken together, these results suggest that cells harboring *KRAS* mutations have an IGF1R pathway with strong basal activity and that this pathway is critical for PI3K activation.

To assess the relative expression levels of known regulators of the IGF1R pathway between the *KRAS*-mutant and wild-type genotypes, we isolated mRNA from the large NSCLC cell panel and conducted quantitative PCR analysis on several components of the pathway, including the genes encoding the receptors (IGF1R, IGF2R, INSR), ligands (IGF1, IGF2), IGF-binding proteins (IGFBPs 1–6), and adaptors (p85α, GRB10, IRS1, and IRS2). The results showed that while levels of most mRNAs were very similar across the different genotypes, *KRAS*-mutant cells expressed modestly higher levels of *IRS1* than wild-type cells. Moreover, although the values did not reach statistical significance, *KRAS*-mutant cells also exhibited increased levels of IRS2 (Fig. 4D and data not shown). Interestingly, analysis of publicly available gene expression data emerging from 2 independent large-scale cancer cell line projects (25, 26) indicates that, in general, expression levels of *IRS1* are elevated in *KRAS*-mutant lung cancer cell lines relative to *KRAS* wild-type comparators (Supplementary Fig. S8D and S8E). In addition, *KRAS*-mutant lung adenocarcinoma tissue samples (27) exhibited increased expression of both *IRS2* and *IGF1R* (Supplementary Fig. S8E). Finally, we analyzed the dependence of the NSCLC cell line panel upon IRS1 and/or IRS2 expression by conducting siRNA-mediated gene knockdown. Depletion of IRS1, IRS2, or both together produced a selective decrease in cell viability, accompanied by an increase in apoptosis in the *KRAS*-mutant cells that was comparable to the effects elicited by control *KRAS* siRNA treatment (Fig. 4E and see also Fig. 1A). These data are consistent with the higher degree of sensitivity of *KRAS*-mutant NSCLC cells to IGF1R inhibition by targeted small molecules and support the notion that *KRAS*-mutant cells display an increased reliance upon IGF1R signaling for their survival.

KRAS Depletion Attenuates AKT Activation in KRAS-Mutant NSCLC Cells

To investigate whether the loss of KRAS expression in lung cancer cells leads to the suppression of PI3K as well as ERK pathway activation, we assessed the impact of KRAS knockdown using 2 different siRNA pools in 12 cell lines, 6 of which are *KRAS* mutant and 6 *KRAS* wild-type. We observed that acute loss of KRAS expression led to a striking reduction in ERK phosphorylation that was much more evident in *KRAS*-mutant cells. In addition, the mutant cells exhibited a similarly strong and selective reduction in S6 phosphorylation. Moreover, we found that KRAS depletion also significantly diminished AKT activation, monitored by phosphorylation of AKT on either Ser473 or Thr308 or PRAS40 on Thr246, preferentially in *KRAS*-mutant NSCLC cells, albeit to a lesser extent than its impact upon phospho-ERK and phospho-S6 (Fig. 5A and Supplementary Fig. S9A).

The fact that mTORC1 activity, as indicated by S6 phosphorylation, is sensitive to MEK inhibition (Fig. 2A) and to KRAS knockdown (Fig. 5A and Supplementary Fig. S9A) in *KRAS*-mutant NSCLC cells suggested that the established negative regulatory feedback loop involving phosphorylation of IRS1 by mTORC1 directly or via S6K1 (28–30) may play a significant role in the control of PI3K activity in these cells. Thus, when MEK and S6K are inhibited following KRAS knockdown, loss of negative feedback means there is a tendency to increase IGF1R signaling via IRS to PI3K/AKT, which counteracts any possible direct impact of KRAS loss on PI3K activation. We therefore sought to assess the effect of inhibiting this feedback loop upon AKT phosphorylation by treating cells with rapamycin in both the presence and absence of KRAS expression. As illustrated in Fig. 5B and Supplementary Fig. S9B, rapamycin treatment of control siRNA-transfected *KRAS*-mutant NSCLC cells increased the levels of phospho-AKT, indicating the presence of an intact feedback loop. Nevertheless, rapamycin was clearly unable to enhance AKT activation following acute depletion of KRAS expression, emphasizing the extent of the KRAS knockdown-induced decrease in AKT activation, even in cell lines such as H1792 where the effect of KRAS knockdown alone is less striking. Taken together, these data suggest that direct interaction of KRAS with p110 may play a critical role in the control of PI3K signaling in NSCLC cells.

Activation of PI3K by Acute Oncogenic RAS Signaling Is Sensitive to IGF1R Inhibition

To look further into the influence of oncogenic RAS activity on IGF1R-mediated survival signaling, we sought to analyze the effect of acute oncogenic RAS activation in untransformed human epithelial cells. To this end, we stably introduced a 4-hydroxytamoxifen (4-OHT)-regulatable oncogenic RAS chimeric protein, ER:HRAS V12 (31), into the spontaneously immortalized breast epithelial cell line MCF10A. The addition of 4-OHT to these cells led to the activation of RAS downstream signaling in a time-dependent fashion, as evidenced by the sustained increase in ERK and AKT phosphorylation (Supplementary Fig. S10A). As anticipated, pretreatment of MCF10A/ER:HRAS V12 cells with MEK inhibitors led to the abrogation of ERK phosphorylation in response to short-term 4-OHT stimulation, with no effect on AKT phosphorylation (Fig. 6A). More notably, pretreatment of the cells with IGF1R inhibitors led to the ablation of residual and 4-OHT–inducible IRS1 phosphorylation, along with a striking inhibition of AKT phosphorylation in response to RAS activation (Fig. 6A). To rule out possible RAS isoform-specific effects, we first established that these observations could be replicated in the same cell system expressing a 4-OHT–activatable ER:KRAS V12 chimeric protein (ref. 10; Supplementary Fig. S10B). Next, to extend our findings to an untransformed lung epithelial cell context, we stably expressed ER:KRAS V12 in NL-20 (32) and type II pneumocyte (33) cells, immortalized human cell lines derived from bronchial and alveolar epithelia, respectively. Figure 6B and C show that the short-term activation of an oncogenic KRAS signal in each of these cell lines led to the marked increase in phosphorylation of ERK and AKT, albeit from a higher basal level than seen in the MCF10A cells. Importantly, as in the MCF10A cell background, pretreatment of the cells with IGF1R inhibitors effectively blocked the 4-OHT–induced phosphorylation of AKT. Finally, to investigate the acute activation of oncogenic RAS signaling in a cancer cell context, we stably

Published OnlineFirst March 1, 2013; DOI: 10.1158/2159-8290.CD-12-0446

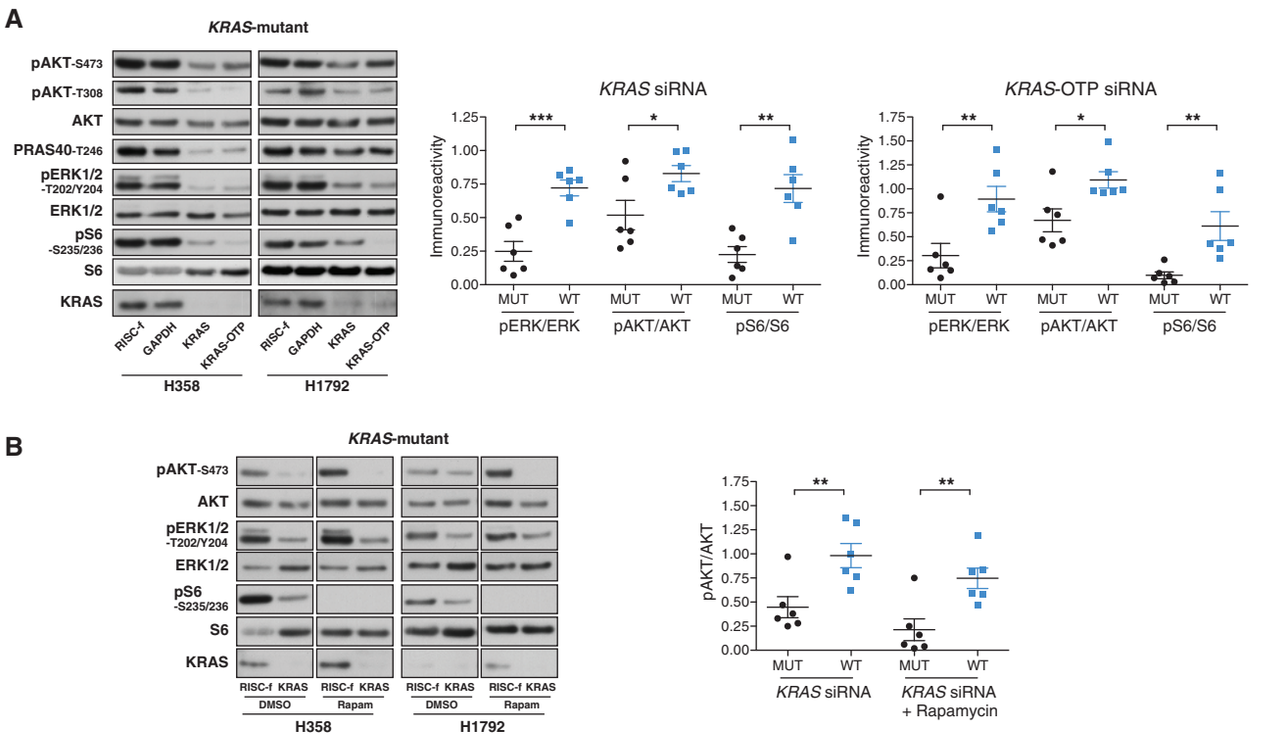

Figure 5. KRAS is required for both MEK/ERK and PI3K/AKT signaling in *KRAS*-mutant NSCLC cells. **A,** six *KRAS*-mutant and 6 *KRAS* wild-type NSCLC cell lines were transfected with *KRAS*, *KRAS*-OTP, or control siRNAs for 48 hours, and cell lysates were probed with the indicated antibodies. The levels of phosphorylated ERK (pERK)/total ERK1/2, AKT, and S6 were measured for each cell line and normalized to control transfected cells. H1792 and H358 cells are displayed as exemplars of the *KRAS*-mutant genotype. For all Western blots, see Supplementary Fig. S9A. **B,** NSCLC cell lines were transfected with KRAS or control siRNAs for 48 hours. Twenty-four hours after transfection cells were treated with either dimethyl sulfoxide (DMSO) or 100 nmol/L rapamycin. Cell lysates were probed with the indicated antibodies. The level of phosphorylated AKT (pAKT)/total AKT was measured for each cell line and normalized to control transfected cells for each condition (+/− rapamycin). H1792 and H358 cells are displayed as exemplars of the *KRAS*-mutant genotype. For all Western blots, see Supplementary Fig. S9B. MUT, mutant; WT, wild-type.

expressed ER:HRAS V12 in the NSCLC cell line SK-MES-1, which is wild-type for *KRAS* and only very modestly sensitive to IGF1R inhibitors. A short 4-hour stimulation of SK-MES-1/ER:HRAS V12 with 4-OHT was also able to induce both ERK and AKT phosphorylation. Moreover, the activation of AKT was again sensitive to prior inhibition of IGF1R, although not completely blocked, whereas ERK activation remained unaffected (Fig. 6D). As shown in Fig. 4B, the phosphorylation of AKT in SK-MES-1 NSCLC cells was also sensitive to inhibition of EGFR by erlotinib. We therefore assessed the effect of pretreating SK-MES-1/ER:HRAS V12 cells with the EGFR inhibitor erlotinib, or a combination of NVP-AEW541 and erlotinib, before 4-OHT induction. Figure 6D illustrates that erlotinib inhibited RAS-induced AKT activation to a similar level as NVP-AEW541, implying a significant input from EGFR as well as IGF1R in these cells. Furthermore, the combination of both of these targeted inhibitors was able to provide a near-complete blockade of AKT phosphorylation in response to 4-OHT. In sum, these observations confirm that inhibition of IGF1R is able to blunt the activation of AKT elicited by acute induction of RAS signaling and further suggest that context-dependent input from other RTKs can also play a notable role. As a whole, our data support the contention that PI3K activation is controlled by coordinate input from RAS proteins and RTKs, and that in *KRAS*-mutant NSCLC the predominant RTK in this regard is the IGF1R (Fig. 6E).

DISCUSSION

In the standard model of RAS-driven tumorigenesis, oncogenic RAS protein is thought to induce the activity of a number of downstream effector enzyme families by direct interaction of GTP-bound RAS with its targets, including RAF kinases, PI3K isoforms, and guanine nucleotide exchange factors for RAL GTPases (4, 34). In the case of type I PI3K, GTP-bound RAS can interact directly with the RAS-binding domain (RBD) on the catalytic p110 subunits (35–39), leading to enzymatic activation. The interaction of RAS.GTP with p110 promotes allosteric activation of PI3K in a manner that is cooperative with signal inputs from RTKs, which act through the binding of tyrosine phosphorylated sequences to the p85 regulatory subunit, relieving its autoinhibitory function (37, 38, 40). The ability of RAS to interact with p110α has been shown to be essential for mutant *Kras*-induced lung cancer formation and mutant *Hras*-induced skin cancer formation in mouse models (41).

The ability of RAS to activate both RAF and PI3K directly has led to great interest in the possibility of treating *RAS*-mutant tumors by inhibiting both pathways in combination.

Published OnlineFirst March 1, 2013; DOI: 10.1158/2159-8290.CD-12-0446

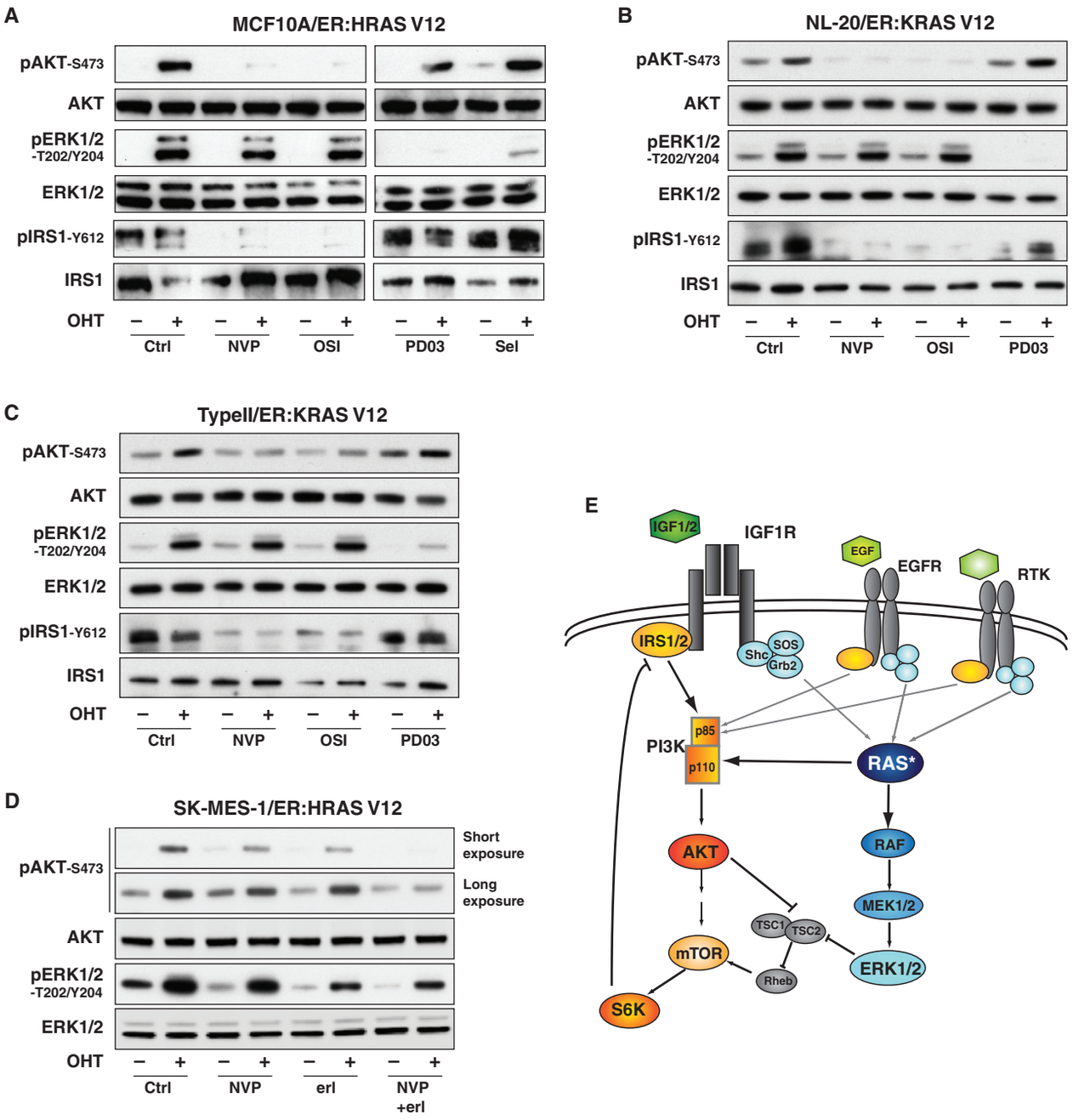

Figure 6. Acute oncogenic RAS signaling is sensitive to IGF1R inhibition. **A,** MCF10A/ER:HRAS V12 cells were deprived of growth factors for 24 hours and treated with vehicle or 100 nmol/L 4-OHT for 4 hours following a 20-minute inhibitor pretreatment. **B** and **C,** NL-20/ER:KRAS V12 (**B**) or Type II/ER:KRAS V12 (**C**) cells were deprived of serum for 24 hours and treated with vehicle or 250 nmol/L 4-OHT for 4 hours following a 20-minute inhibitor pretreatment. **D,** SK-MES-1/ER:HRAS V12 cells were deprived of serum for 24 hours and treated with vehicle or 100 nmol/L 4-OHT for 4 hours following a 20-minute inhibitor pretreatment. **A–D,** inhibitor treatment: DMSO (Ctrl), 1 μmol/L NVP-AEW541, 1 μmol/L OSI-906, 5 nmol/L PD-0325901, 90 nmol/L selumetinib, or 1 μmol/L erlotinib. Cell lysates were probed with the indicated antibodies. **E,** model of PI3K activation by oncogenic RAS and RTK signaling in *KRAS*-mutant NSCLC cells.

Published OnlineFirst March 1, 2013; DOI: 10.1158/2159-8290.CD-12-0446

The use of PI3K and MEK inhibitors in a mouse model of *Kras*-induced lung cancer has provided support for this idea (8). However, although it has been shown that, once established, *RAS*-mutant cancers show dependence on PI3K signaling for tumor maintenance (42), it is not yet clear whether this is due to direct RAS–PI3K interaction or some more indirect mechanism. It is also not certain that *RAS*-mutant cancer cells show any greater degree of dependence on PI3K signaling than do cells with other genotypes, raising the issue of whether or not PI3K inhibitors will have a useful therapeutic window in the treatment of *RAS*-mutant cancers. We therefore undertook the drug screening approach described here to look for agents with selectivity for *RAS*-mutant relative to *RAS* wild-type lung cancer cell lines. The results show that while PI3K inhibition was toxic to cultured *RAS*-mutant cells, it was not obviously any more selective for cells with *RAS* mutations compared to cells with other genotypes. This is in contrast to the finding that RAF/MEK/ERK pathway function is indeed selectively required by *RAS*-mutant cells, as has been described with increasing certainty by others in recent years (16, 25, 26, 43, 44). In addition, we unexpectedly found that *RAS*-mutant lung cancer cell lines very clearly showed heightened sensitivity to RTK inhibitors targeting the IGF1 receptor. It is worth noting that these *KRAS*-mutant genotype-specific effects of RAF/MEK and IGF1R inhibition are also present in data available from the Genomics of Drug Sensitivity in Cancer project from the Wellcome Trust Sanger Institute (Cambridgeshire, United Kingdom; ref. 26), based on large-scale drug screening of several hundred cell lines derived from a broad range of tissue types: mutant *KRAS* selectivity is seen with AZ628 (RAF inhibitor), PD-0325901, selumetinib and RDEA119 (MEK inhibitors), and BMS-754807 and OSI-906 (IGF1R inhibitors).

A study of *KRAS*-mutant colon cancer cell lines recently reported a clear tendency toward sensitivity to IGF1R inhibition (45). In this work, as in our work on *KRAS*-mutant lung cancer cell lines, *RAS*-mutant cells showed good sensitivity to combinations of MEK and IGF1R inhibitors, and there were indications that basal PI3K signaling was dependent on signaling flux through IGF1R to IRS1/IRS2 to p85/p110. However, while the therapeutic implications of our work and that of Ebi and colleagues (46) are similar, different mechanistic interpretations were made. In contrast to our analysis here, Ebi and colleagues did not see a negative impact of removal of *KRAS* by RNAi knockdown on PI3K activity in *KRAS*-mutant cells. The basis for this difference is unclear. One possibility is that it reflects the differing tissue types of origin of the cells; the frequency of coincident mutation of *KRAS* and *PIK3CA* in colon but not lung cancer suggests that there might be significant differences in the interplay between these signaling systems in the 2 tissues. A quantitative model of RAS signaling to PI3K concludes that the relative contributions of RAS and RTKs to PI3K activation depend strongly on the quantities and binding affinities of the interacting proteins, which are likely to vary greatly across different cell types and stimuli (46). Alternatively, this might reflect differences in the efficiency of *KRAS* knockdown between the short hairpin RNA (shRNA) and siRNA approaches used. It is possible that RAS protein expression has to be reduced below different thresholds to have an impact on RAF and on PI3K signaling. The tendency of MEK and mTOR inhibition to cause PI3K activation due to relief of negative feedback onto IRS1 can also obscure the direct impact of loss of RAS expression on PI3K activity, which can be revealed when mTOR activity is artificially inhibited by rapamycin, as shown in Fig. 5.

The use of a posttranslationally activatable form of oncogenic RAS allows more precise probing of the role of RAS in PI3K regulation, including in a time frame that will be minimally affected by RAS pathway–induced changes in gene expression. From this, it is clear that short-term RAS activation can result in stimulation of PI3K, but that this is dependent on input from the IGF1R tyrosine kinase. It is thus likely that RAS requires relief of the inhibitory effect of the unliganded p85 regulatory subunit of PI3K (47) to be able to effectively activate its lipid kinase activity through direct RAS–p110 interaction, and that, in *KRAS*-mutant lung cancer, this signaling input into p85 is provided by basal IGF1R signaling. This effect was seen in untransformed immortalized breast epithelial cells and also in 2 different cultures of normal immortalized lung epithelial cells with posttranslationally inducible RAS activity. We also tested this in an NSCLC line lacking *KRAS* mutation. Although this showed dependence of RAS-induced PI3K pathway activation on IGF1R function, there was also a component of EGFR dependence. It is likely that this reflects the mixed IGF1R and EGFR dependence of the parental *KRAS* wild-type SK-MES-1 cell line, whereas the *KRAS*-mutant NSCLC lines seem to be much more dependent on IGF1R rather than EGFR signaling (Fig. 4B). We speculate that in this inducible system, acutely activated RAS will use input from whatever basally active RTK is present in the cells to relieve p85 mediated autoinhibition of PI3K activity; in *KRAS*-mutant NSCLC this is predominantly IGF1R, whereas in *KRAS* wild-type NSCLC both IGF1R and EGFR contribute.

The findings described here using cultured lung cancer cell lines and also mouse lung cancer models suggest that there may be value to the use of combinations of MEK and IGF1R inhibitors to treat patients with *KRAS*-mutant lung cancer. The work reported here has used small-molecule kinase inhibitors that target both IGF1R and the related insulin receptor; further work will be required to determine the relative merits in this context of these inhibitors compared with IGF1R-directed monoclonal antibodies, which generally do not target the insulin receptor. In comparison with PI3K inhibitors, IGF1R inhibitors seem to have less single-agent impact on *KRAS* wild-type cells, suggesting that these agents might show less toxicity *in vivo*. However, to date, IGF1R inhibitors have not shown great promise as single agents in clinical trials, with the exception of on some sarcomas (48). With the MEK inhibitor trametinib clearly now an attractive candidate for the treatment of *KRAS*-mutant NSCLC, our work suggests that early combination with an IGF1R inhibitor may be beneficial.

METHODS

Cell Lines and Culture

MCF10A/ER:HRAS V12 and SK-MES-1/ER:HRAS V12 cells were constructed by transducing parental MCF10A breast epithelial cells or SK-MES-1 NSCLC cells with a bleocin-resistant retrovirus

Published OnlineFirst March 1, 2013; DOI: 10.1158/2159-8290.CD-12-0446

encoding the murine ecotropic receptor. Selected cells were subsequently infected with puromycin-resistant ER:HRAS V12 retrovirus (31). MCF10A/ER:KRAS V12, NL-20/ER:KRAS V12 and TypeII/ER:KRAS V12 were constructed by transducing parental MCF10A, NL-20, or TypeII cells with pLenti-PGK-ER-KRAS(G12V) (Haber lab Addgene plasmid no. 35635) and selecting under hygromycin. Detailed origin and growing conditions of all cell lines used are given in the Supplementary Material. Cell lines were authenticated by the Cancer Research UK Central Cell Services facility using short tandem repeat profiling.

siRNA Reagents and Cell Viability Assays

All siRNAs were obtained from Dharmacon and were used as "SMARTpools" according to the manufacturer's instructions. Viability assays following siRNA transfection experiments or the addition of small-molecule inhibitors were conducted in 96-well format as previously described (12). Starting cell density was optimized to produce an 80% confluent monolayer in mock-treated cells at the conclusion of the experiment. Cell viability was determined using Cell Titer Blue (Promega), and apoptosis induction was recorded using a caspase-3/7 consensus site peptide (Z-DEVD)2 conjugated to rhodamine 110 (Invitrogen; ref. 12). For long-term drug treatments, cells were seeded in 12-well format for 24 hours and treated with drugs for 12 days. Cells were fixed with 2% paraformaldehyde, stained with 0.2% crystal violet, and finally dissolved with acetic acid. Absorbance was measured at 595 nm. Detailed information on the small inhibitors used is given in the Supplementary Material.

Western Blotting

For quantitative Western blotting, bound primary antibodies were detected by secondary conjugates compatible with infrared detection at 700 nm and 800 nm, and membranes were scanned using the Odyssey Infrared Imaging System (Odyssey, LICOR). Alternatively, membranes were incubated with horseradish peroxidase-conjugated secondary antibody, detected using chemiluminescence (Millipore), and quantified using Image Quant LAS4000 (GE Healthcare). Detailed information on the antibodies used is given in the Supplementary Material.

Co-Immunoprecipitations

Cells growing under steady-state conditions were scraped into ice-cold lysis buffer comprising 25 mmol/L Tris pH 7.6, 150 mmol/L NaCl, 0.5% Nonidet P-40, 0.5 mmol/L DTT, 1 mmol/L EDTA, 1 mmol/L EGTA, 0.5 mmol/L phenylmethylsulfonylfluoride, 10 μg/mL leupeptin, 5 μg/mL aprotinin, 50 mmol/L NaF, 1 mmol/L sodium vanadate, 10 mmol/L β–glycerophosphate, and 10 mmol/L sodium pyrophosphate. Following a short incubation on ice, lysates were centrifuged at 20,000 × *g* for 5 minutes at 4°C and the supernatants used for immunoprecipitation using anti-p85α antibody. Immunoprecipitates were washed 3 times with ice-cold lysis buffer before boiling in sample buffer.

Quantitative RT-PCR

RNA was isolated (Qiagen) and reverse transcription was conducted (Applied Biosystems) using standard methods. Quantitative real-time PCR was conducted using gene-specific primers (QuantiTect Primer Assays, Qiagen) for *IGF1R, IRS1, IRS2, p85α,* or *18S* with Fast SYBR Green Master Mix (Applied Biosystems).

Mouse Experiments

Kras$^{LSL\text{-}G12D}$; *Trp53*$^{Flox/Flox}$ mice and *Kras*$^{LA2\text{-}G12D/+}$ mice were from the Mouse Models of Human Cancer Consortium (23, 49). *Kras*$^{LSL\text{-}G12D}$; *Trp53*$^{Flox/Flox}$ mice were infected with adenovirus expressing Cre recombinase as described (50). Sixteen-week-old *Kras*$^{LSL\text{-}G12D}$; *Trp53*$^{Flox/Flox}$ mice; and 12-week-old *Kras*$^{LA2\text{-}G12D/+}$ mice were treated for 2 or 6 weeks, respectively, by oral gavage delivery of vehicle, MEK inhibitor (2.5 mg/kg/d trametinib), IGF1R inhibitor (40 mg/kg/d OSI-906 or 50 mg/kg/d NVP-AEW541), or both drugs together. Micro-CT analysis was conducted using the SkyScan 1176. Mice were scanned pre- and postdrug treatment regimes. Micro-CT data were sorted, processed, and reconstructed using the N-Recon (SkyScan). Reconstructed data were subsequently imaged using DataViewer, and tumor volumes were calculated using the CTan program (SkyScan).

Data Analysis

Data are presented as mean ± SD unless otherwise stated. For viability and Western blot quantifications, significance was assessed with the 2-tailed unpaired *t* test. For apoptosis and gene expression analysis, significance was determined using the Mann–Whitney U test. For correlation analyses, Pearson coefficient was used. Comparison between 2 viability curves was done using 2-way ANOVA. The level of significance was set at $P < 0.05$ (*), $P < 0.01$ (**), and $P < 0.001$ (***). The CalcuSyn program (Biosoft), which uses the combination index equation of Chou–Talalay, was used to determine likely synergy of drug combinations using fixed drug ratios.

Disclosure of Potential Conflicts of Interest

No potential conflicts of interest were disclosed.

Authors' Contributions

Conception and design: M. Molina-Arcas, D.C. Hancock, J. Downward
Development of methodology: D.C. Hancock, M.S. Kumar
Acquisition of data (provided animals, acquired and managed patients, provided facilities, etc.): M. Molina-Arcas, D.C. Hancock, C. Sheridan, M.S. Kumar
Analysis and interpretation of data (e.g., statistical analysis, biostatistics, computational analysis): M. Molina-Arcas, D.C. Hancock, C. Sheridan
Writing, review, and/or revision of the manuscript: M. Molina-Arcas, D.C. Hancock, J. Downward
Administrative, technical, or material support (i.e., reporting or organizing data, constructing databases): D.C. Hancock
Study supervision: J. Downward

Acknowledgments

The authors thank Markus Diefenbacher, Ralph Fritsch, Michael Steckel, Gavin Kelly, Emma Nye, and Gordon Stamp for assistance and discussion.

Grant Support

This work was supported by Cancer Research UK and by the European Union Framework Programme 7 "LUNGTARGET" consortium grant.

Received October 1, 2012; revised February 20, 2013; accepted February 21, 2013; published OnlineFirst March 1, 2013.

REFERENCES

1. Ferlay J, Shin HR, Bray F, Forman D, Mathers C, Parkin DM. Estimates of worldwide burden of cancer in 2008: GLOBOCAN 2008. Int J Cancer 2010;127:2893–917.
2. Ding L, Getz G, Wheeler DA, Mardis ER, McLellan MD, Cibulskis K, et al. Somatic mutations affect key pathways in lung adenocarcinoma. Nature 2008;455:1069–75.

Published OnlineFirst March 1, 2013; DOI: 10.1158/2159-8290.CD-12-0446

3. Heist RS, Engelman JA. SnapShot: non-small cell lung cancer. Cancer Cell 2012;21:448.
4. Downward J. Targeting RAS signalling pathways in cancer therapy. Nat Rev Cancer 2003;3:11–22.
5. Pylayeva-Gupta Y, Grabocka E, Bar-Sagi D. RAS oncogenes: weaving a tumorigenic web. Nat Rev Cancer 2011;11:761–74.
6. Torti D, Trusolino L. Oncogene addiction as a foundational rationale for targeted anti-cancer therapy: promises and perils. EMBO Mol Med 2011;3:623–36.
7. Singh A, Greninger P, Rhodes D, Koopman L, Violette S, Bardeesy N, et al. A gene expression signature associated with "K-Ras addiction" reveals regulators of EMT and tumor cell survival. Cancer Cell 2009;15:489–500.
8. Engelman JA, Chen L, Tan X, Crosby K, Guimaraes AR, Upadhyay R, et al. Effective use of PI3K and MEK inhibitors to treat mutant Kras G12D and PIK3CA H1047R murine lung cancers. Nat Med 2008;14:1351–6.
9. Barbie DA, Tamayo P, Boehm JS, Kim SY, Moody SE, Dunn IF, et al. Systematic RNA interference reveals that oncogenic KRAS-driven cancers require TBK1. Nature 2009;462:108–12.
10. Singh A, Sweeney MF, Yu M, Burger A, Greninger P, Benes C, et al. TAK1 inhibition promotes apoptosis in KRAS-dependent colon cancers. Cell 2012;148:639–50.
11. Kumar MS, Hancock DC, Molina-Arcas M, Steckel M, East P, Diefenbacher M, et al. The GATA2 Transcriptional Network Is Requisite for RAS Oncogene-Driven Non-Small Cell Lung Cancer. Cell 2012;149:642–55.
12. Steckel M, Molina-Arcas M, Weigelt B, Marani M, Warne PH, Kuznetsov H, et al. Determination of synthetic lethal interactions in KRAS oncogene-dependent cancer cells reveals novel therapeutic targeting strategies. Cell Res 2012;22:1227–45.
13. Puyol M, Martin A, Dubus P, Mulero F, Pizcueta P, Khan G, et al. A synthetic lethal interaction between K-Ras oncogenes and Cdk4 unveils a therapeutic strategy for non-small cell lung carcinoma. Cancer Cell 2010;18:63–73.
14. Luo J, Emanuele MJ, Li D, Creighton CJ, Schlabach MR, Westbrook TF, et al. A genome-wide RNAi screen identifies multiple synthetic lethal interactions with the Ras oncogene. Cell 2009;137:835–48.
15. Jackson AL, Burchard J, Leake D, Reynolds A, Schelter J, Guo J, et al. Position-specific chemical modification of siRNAs reduces "off-target" transcript silencing. RNA 2006;12:1197–205.
16. Solit DB, Garraway LA, Pratilas CA, Sawai A, Getz G, Basso A, et al. BRAF mutation predicts sensitivity to MEK inhibition. Nature 2006;439:358–62.
17. Khazak V, Astsaturov I, Serebriiskii IG, Golemis EA. Selective Raf inhibition in cancer therapy. Expert Opin Ther Targets 2007;11:1587–609.
18. Chandarlapaty S. Negative feedback and adaptive resistance to the targeted therapy of cancer. Cancer Discov 2012;2:311–9.
19. Ma L, Chen Z, Erdjument-Bromage H, Tempst P, Pandolfi PP. Phosphorylation and functional inactivation of TSC2 by Erk implications for tuberous sclerosis and cancer pathogenesis. Cell 2005;121:179–93.
20. Roux PP, Ballif BA, Anjum R, Gygi SP, Blenis J. Tumor-promoting phorbol esters and activated Ras inactivate the tuberous sclerosis tumor suppressor complex via p90 ribosomal S6 kinase. Proc Natl Acad Sci U S A 2004;101:13489–94.
21. Gilmartin AG, Bleam MR, Groy A, Moss KG, Minthorn EA, Kulkarni SG, et al. GSK1120212 (JTP-74057) is an inhibitor of MEK activity and activation with favorable pharmacokinetic properties for sustained *in vivo* pathway inhibition. Clin Cancer Res 2011;17:989–1000.
22. Flaherty KT, Robert C, Hersey P, Nathan P, Garbe C, Milhem M, et al. Improved survival with MEK inhibition in BRAF-mutated melanoma. N Engl J Med 2012;367:107–14.
23. Johnson L, Mercer K, Greenbaum D, Bronson RT, Crowley D, Tuveson DA, et al. Somatic activation of the K-ras oncogene causes early onset lung cancer in mice. Nature 2001;410:1111–6.
24. Jackson EL, Olive KP, Tuveson DA, Bronson R, Crowley D, Brown M, et al. The differential effects of mutant p53 alleles on advanced murine lung cancer. Cancer Res 2005;65:10280–8.
25. Barretina J, Caponigro G, Stransky N, Venkatesan K, Margolin AA, Kim S, et al. The Cancer Cell Line Encyclopedia enables predictive modelling of anticancer drug sensitivity. Nature 2012;483:603–7.
26. Garnett MJ, Edelman EJ, Heidorn SJ, Greenman CD, Dastur A, Lau KW, et al. Systematic identification of genomic markers of drug sensitivity in cancer cells. Nature 2012;483:570–5.
27. Bild AH, Yao G, Chang JT, Wang Q, Potti A, Chasse D, et al. Oncogenic pathway signatures in human cancers as a guide to targeted therapies. Nature 2006;439:353–7.
28. Tzatsos A, Kandror KV. Nutrients suppress phosphatidylinositol 3-kinase/Akt signaling via raptor-dependent mTOR-mediated insulin receptor substrate 1 phosphorylation. Mol Cell Biol 2006;26:63–76.
29. Harrington LS, Findlay GM, Gray A, Tolkacheva T, Wigfield S, Rebholz H, et al. The TSC1-2 tumor suppressor controls insulin-PI3K signaling via regulation of IRS proteins. J Cell Biol 2004;166:213–23.
30. Shah OJ, Wang Z, Hunter T. Inappropriate activation of the TSC/Rheb/mTOR/S6K cassette induces IRS1/2 depletion, insulin resistance, and cell survival deficiencies. Curr Biol 2004;14:1650–6.
31. Dajee M, Tarutani M, Deng H, Cai T, Khavari PA. Epidermal Ras blockade demonstrates spatially localized Ras promotion of proliferation and inhibition of differentiation. Oncogene 2002;21:1527–38.
32. Schiller JH, Bittner G. Loss of the tumorigenic phenotype with *in vitro*, but not *in vivo*, passaging of a novel series of human bronchial epithelial cell lines: possible role of an alpha 5/beta 1-integrin-fibronectin interaction. Cancer Res 1995;55:6215–21.
33. Kemp SJ, Thorley AJ, Gorelik J, Seckl MJ, O'Hare MJ, Arcaro A, et al. Immortalization of human alveolar epithelial cells to investigate nanoparticle uptake. Am J Respir Cell Mol Biol 2008;39:591–7.
34. Repasky GA, Chenette EJ, Der CJ. Renewing the conspiracy theory debate: does Raf function alone to mediate Ras oncogenesis? Trends Cell Biol 2004;14:639–47.
35. Kodaki T, Woscholski R, Hallberg B, Rodriguez-Viciana P, Downward J, Parker PJ. The activation of phosphatidylinositol 3-kinase by Ras. Curr Biol 1994;4:798–806.
36. Rodriguez-Viciana P, Warne PH, Dhand R, Vanhaesebroeck B, Gout I, Fry MJ, et al. Phosphatidylinositol-3-OH kinase as a direct target of Ras. Nature 1994;370:527–32.
37. Pacold ME, Suire S, Perisic O, Lara-Gonzalez S, Davis CT, Walker EH, et al. Crystal structure and functional analysis of Ras binding to its effector phosphoinositide 3-kinase gamma. Cell 2000;103:931–43.
38. Suire S, Hawkins P, Stephens L. Activation of phosphoinositide 3-kinase gamma by Ras. Curr Biol 2002;12:1068–75.
39. Yang HW, Shin MG, Lee S, Kim JR, Park WS, Cho KH, et al. Cooperative activation of PI3K by Ras and Rho family small GTPases. Mol Cell 2012;47:281–90.
40. Rodriguez-Viciana P, Warne PH, Vanhaesebroeck B, Waterfield MD, Downward J. Activation of phosphoinositide 3-kinase by interaction with Ras and by point mutation. EMBO J 1996;15:2442–51.
41. Gupta S, Ramjaun AR, Haiko P, Wang Y, Warne PH, Nicke B, et al. Binding of ras to phosphoinositide 3-kinase p110alpha is required for ras-driven tumorigenesis in mice. Cell 2007;129:957–68.
42. Lim KH, Counter CM. Reduction in the requirement of oncogenic Ras signaling to activation of PI3K/AKT pathway during tumor maintenance. Cancer Cell 2005;8:381–92.
43. McCubrey JA, Steelman LS, Abrams SL, Chappell WH, Russo S, Ove R, et al. Emerging MEK inhibitors. Expert Opin Emerg Drugs 2010;15:203–23.
44. Collisson EA, Trejo CL, Silva JM, Gu S, Korkola JE, Heiser LM, et al. A central role for RAF->MEK->ERK signaling in the genesis of pancreatic ductal adenocarcinoma. Cancer Discov 2012;2:685–93.

Published OnlineFirst March 1, 2013; DOI: 10.1158/2159-8290.CD-12-0446

45. Ebi H, Corcoran RB, Singh A, Chen Z, Song Y, Lifshits E, et al. Receptor tyrosine kinases exert dominant control over PI3K signaling in human KRAS mutant colorectal cancers. J Clin Invest 2011;121:4311–21.
46. Kaur H, Park CS, Lewis JM, Haugh JM. Quantitative model of Ras-phosphoinositide 3-kinase signalling cross-talk based on co-operative molecular assembly. Biochem J 2006;393:235–43.
47. Kok K, Geering B, Vanhaesebroeck B. Regulation of phosphoinositide 3-kinase expression in health and disease. Trends Biochem Sci 2009;34:115–27.
48. Scagliotti GV, Novello S. The role of the insulin-like growth factor signaling pathway in non-small cell lung cancer and other solid tumors. Cancer Treat Rev 2012;38:292–302.
49. Jackson EL, Willis N, Mercer K, Bronson RT, Crowley D, Montoya R, et al. Analysis of lung tumor initiation and progression using conditional expression of oncogenic K-ras. Genes Dev 2001;15:3243–8.
50. DuPage M, Dooley AL, Jacks T. Conditional mouse lung cancer models using adenoviral or lentiviral delivery of Cre recombinase. Nat Protoc 2009;4:1064–72.

Published OnlineFirst March 1, 2013; DOI: 10.1158/2159-8290.CD-12-0446

AACR American Association for Cancer Research

CANCER DISCOVERY

Coordinate Direct Input of Both KRAS and IGF1 Receptor to Activation of PI3 kinase in *KRAS*-Mutant Lung Cancer

Miriam Molina-Arcas, David C. Hancock, Clare Sheridan, et al.

Cancer Discovery 2013;3:548-563. Published OnlineFirst March 1, 2013.